Filling holes using a mesh of filled curves

M. A. Fortes[a], P. González[a], A. Palomares[a], M. L. Rodríguez[a,*]

[a]*Departamento de Matemática Aplicada. Universidad de Granada. Edificio Politécnico. C/ Severo Ochoa, s/n. 18071 Granada (Spain)*

Abstract

The objective of this work is to fill graphics of surfaces with holes-meeting shape conditions, i. e., we want to determine values of a surface inside a hole -where it is not defined- by means of its values outside the hole -where it is properly defined- in such a way that the final reconstructed surface be fair and smooth enough. The procedure considered to get this aim is based on a one-dimensional hole-filling problem, leading to a kind of "wireframe" surface. We develop the theoretical aspects of the problem and we show some graphical examples to illustrate the proposed method.

Keywords: Filling holes, Minimal energy, Wireframe surface, Powell-Sabin approximation, Reconstruction.
2010 MSC: 00-01, 99-00

1. Introduction

The problem of interpolating incomplete meshes (hole-filling) and reconstructing surfaces from point clouds derived from 3D range scanners arises in computer graphics and Computer Aided Design (CAD), with applications in e.g. earth sciences, computer vision in robotics and image reconstruction.

There are quite a lot of practical applications where it is indispensable to reconstruct and to fill missed data on a hidden surface or volume from scattered data points. Among these practical applications we can for example highlight, by its economic importance: the oil and gas reservoir detection, the estimated sizing of fish banks and other marine reserves, the situation and layering of tectonic faults or some specific material strata (with high-Z values, like lead, tungsten or gold), the micro-gravimetric prospection for caves and holes detection, the isolation of nuclear combustible and other radioactive wastes, etc. We can also

*Corresponding author
Email address: {mafortes,prodelas,anpalom,miguelrg}@ugr.es (M. L. Rodríguez)

mention the usual radio-frequency seismic and acoustic or electro-magnetic waves, or even some modern techniques using special lasers or even muons, or other cosmic rays, used in some environmental and archaeological tomographies. The most fundamental cause of holes is occlusion - recesses too deep to be observed using a particular triangulation angle.

In the existing literature, several works have paid attention to the "reconstruction" of data (hole-filling), developing methods based on the introduction of different measures and techniques to optimize -commonly minimize- them. Among these works, we can distinguish between reconstruction algorithms that work on connected meshes of range samples and algorithms that operate on clouds of unorganized 3D points. We can highlight the following ones: In [1], the authors use polyharmonic Radial Basis Functions (RBF's) to reconstruct smooth surfaces from point clouds data and to repair incomplete meshes. In [2], the basic principle is to choose the completing surface as the one minimizing a power of the mean curvature. The surface is represented in implicit form and an energy functional for the embedding function is constructed. In [3], the author obtains curves that can be modeled as the solutions of a system of boundary value problems of Ordinary Differential Equations (ODE's). The advantages of the ODE approaches are the optimal blending curves obtained, with minimum energy and flexibility, to complicated blending problems. Another method for reconstructing a polygonal hole based on the minimization of an energy functional, with applications to resolution of elliptic problems, is developed in [4].

On the other hand, several researchers have already tested some ideas regarding the problem of constructing smooth fillings for holes, which is known as the $n-$sided hole problem, from different points of view. Among others, in [5] the author handles the problem of filling polygonal holes with rectangular patches meeting at a common vertex and joining them with geometric continuity. A similar approach has been taken in [6], where the authors use $\mathcal{C}^1$ cubic triangular spline patches for the same proposal. In [7] the authors describe a method that generates a surface into which a n-sided patch (the hole) is inserted. Such a surface is required to be bicubic and of locally uniform parametrization, with $\mathcal{C}^1$ continuity, rather than a B-spline surface. So, it is only needed to specify the n-sided hole to be filled and the localization of some points. In [8] we find a different way of handling this problem: the author builds free-form surfaces with the help of and CAD program and Bernstein patches in three steps. Finally, we want to point out that several manuals ([9, 10, 11]) can be consulted for a thorough treatment of different techniques for the design of surfaces.

The procedure considered in this paper presents a surface reconstruction and hole-filling scheme, based on a beam of parallel and/or orthogonal curves (hereafter called *wireframes*), where previously some specific one-dimensional curve reconstructions have been accomplished inside the hole that we want to fill. Un-

der this perspective, we face the problem of filling a surface by mixing the models presented in [3] and [4] in an efficient way. Instead of addressing the problem as a whole, which yields to a very complicated computational frame, we generate the reconstructed filled surface through one-dimensional filling curves subsequently used to generate the global filling smooth surface. It should be clarify that the method we propose in this paper is developed just for explicit surfaces (i. e., the graphics of functions $f : D \to \mathbb{R}$ defined on a domain $D \subset \mathbb{R}^2$). A generalization of the method with the aim to fill more fgeneral surfaces could be developed following a frame similar to the one considered in [12].

We propose a four-stage procedure to solve the above-mentioned problem. These stages have great flexibility, which allows us to modify certain parameters appearing in the process in order to model some characteristics of the constructed surface.

The first step consists in determining a set of segments on the surface domain such that all of them cross the hole. Secondly, we consider the one-dimensional curves contained in the original surface graphic whose projections onto the domain plane are the segments fixed in the previous step. In the next step, we fill such univariate functions by using different criteria. These criteria are established taking into account that the curves have certain characteristics that come from the surface where they are embedded. Certainly, many different one dimensional reconstruction procedures (using polynomials of different degrees and satisfying different conditions) could be applied, and all of them would produce different –more or less appropriate– ways of filling the hole in the reconstructed surface. In each particular example, this issue is another important subject that can be explored, i. e., depending on the concrete shape of the surface given outside the hole or even on the shape we may want the reconstructed surface inside the hole to have, we could think considering different $1D$-filling schemes. In order to prepare the examples considered in the final section of the paper, we have explored several of them, but we only present two -the quintic one, which reveals to be the better for the test functions considered, and a mixed fitting-interpolation filling criteria-. Finally, we construct a bidimensional function approximating all the univariate filled functions previously obtained. The chosen technique in this final step is based on the minimization of an energy functional where several parameters, which can be modified attending to the geometric conditions to be fulfilled, are involved.

It is important to note that the different steps of *filling the univariate curves* to later obtain the *filling surface from such filled curves* enjoy a measure of independence. Namely, we have the freedom to decide which the $1D$-filling criteria may be to later, independently, obtain the filling surface fitting such filled curves.

The outline of the paper is as follows. In Section 2 we present a brief review of the needed background. Section 3 is devoted to the formulation of the

problem and the statement and proof of the main theoretical results. Finally, we present several graphical and numerical examples to show the performance of the proposed method in the last section.

2. Preliminaries

2.1. Functional spaces

Let $D \subset \mathbb{R}^2$ be a polygonal domain (an open, non-empty connected set) in such a way that $\overline{D}$ admits a Δ^1-type triangulation (Figure 1), defined as the ones induced by integer translates of $x = 0, y = 0$ and $x + y = 0$ (see e.g. [13]).

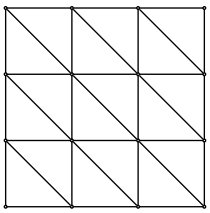

Figure 1: Example of Δ^1-type triangulation.

Let us consider the Sobolev space $\mathcal{H}^2(D)$, whose elements are (classes of) functions u defined on D such that their partial derivatives (in the distribution sense) $\partial^\beta u$ belong to $L^2(D)$, with $\beta := (\beta_1, \beta_2) \in \mathbb{N}^2$ and $|\beta| := \beta_1 + \beta_2 \leq 2$. For any open subset $X \subset D$ we consider the usual inner semi-products

$$(u, v)_{m,X} := \sum_{|\beta|=m} \int_X \partial^\beta u(x) \partial^\beta v(x) dx, \quad m = 0, 1, 2;$$

the semi-norms

$$|u|_{m,X} := (u, u)_{m,X}^{1/2} = \left(\sum_{|\beta|=m} \int_X \partial^\beta u(x)^2 dx \right)^{1/2}, \quad m = 0, 1, 2;$$

and the norm

$$\|u\|_X = \left(\sum_{m=0}^{2} |u|_{m,X}^2 \right)^{1/2} = \left(\sum_{|\beta|\leq 2} \int_X \partial^\beta u(x)^2 dx \right)^{1/2}.$$

We will denote $< \cdot >_n$ the usual Euclidean norm and $< \cdot \, , \, \cdot >_n$ the Euclidean inner product in $\mathbb{R}^n$.

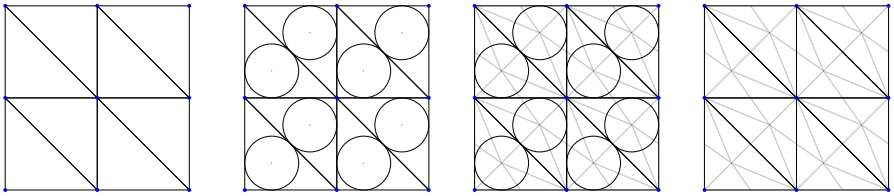

Figure 2: Powell-Sabin sub-triangulation.

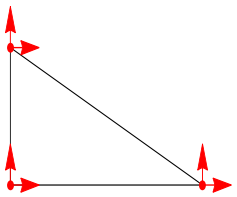

Figure 3: Powell-Sabin finite element data.

2.2. Powell-Sabin triangulation

Given a Δ^1-triangulation of $\overline{D}$, we will consider the associated Powell-Sabin triangulation $\mathcal{T}_6$ of $\mathcal{T}$ (see e.g. [14]), which can be obtained by joining an appropriate interior point Ω_T of each $T \in \mathcal{T}$ to the vertices of T and to the interior points $\Omega_{T'}$ of the neighbouring triangles $T' \in \mathcal{T}$ of T. When T has a side lying on the boundary of D, the point Ω_T is joined to the mid-point of this side, to the vertices of T and to the interior points $\Omega_{T'}$ of the neighbouring triangles $T' \in \mathcal{T}$ of T. Hence, the six micro-triangles inside any $T \in \mathcal{T}$ have the point Ω_T as a common vertex. There are several ways to consider appropriate points Ω_T ([15]), nevertheless, a good choice ([16]) is considering Ω_T to be the incenter of T, for all $T \in \mathcal{T}$ (Figure 2).

Let $\mathcal{Z}_\mathcal{T}$ denotes the set of all vertices of $\mathcal{T}$.

Remark 1. *It is well known ([15]) that given the values of a function f (defined on $\overline{D}$) and the ones of all its first partial derivatives at all the points of $\mathcal{Z}_\mathcal{T}$ (see Figure 3), there exists a unique S in the spline space*

$$\mathcal{S}_2^1(D, \mathcal{T}_6) = \left\{ S \in \mathcal{C}^1(D) : S|_{T'} \in \mathbb{P}_2(T') \quad \forall T' \in \mathcal{T}_6 \right\},$$

where $\mathbb{P}_2$ stands for the space of bivariate polynomials of total degree at most two, such that the values of S and the ones of all its first partial derivatives coincide with those of f at all the points of $\mathcal{Z}_\mathcal{T}$.

Finally, let us recall that the *diameter* of a Δ^1-type triangulation $\mathcal{T}$ of $\overline{D}$ is defined as

$$diam(\mathcal{T}) = \max_{x,y \in T} \|x - y\| \text{ for any } T \in \mathcal{T}.$$

2.3. Data approximation problem

Given a finite set of points $\mathcal{P} = \{p_1, \ldots, p_q\}$ in D and a vector $\mathcal{Z} = (z_1, \ldots, z_q) \in \mathbb{R}^q$, we are interested in finding a $\mathcal{C}^1$-quadratic surface in $\mathcal{S}_2^1(D, \mathcal{T}_6)$ that approximates the points $\{(p_i, z_i)\}_{i=1}^q \subset \mathbb{R}^3$ and minimizes the *functional energy* defined on $\mathcal{S}_2^1(D, \mathcal{T}_6)$ by

$$\mathcal{J}(v) =< \rho(v) - \mathcal{Z} >_q^2 + \tau_1 |v|_{1,D}^2 + \tau_2 |v|_{2,D}^2,$$

where ρ is the *evaluation operator*

$$\begin{array}{rccl} \rho: & \mathcal{S}_2^1(D, \mathcal{T}_6) & \to & \mathbb{R}^q \\ & v & \mapsto & \rho(v) = (v(p_1), \ldots, v(p_q)), \end{array} \tag{1}$$

$\tau_1 \geq 0$ and $\tau_2 > 0$.

Observe that the first term of $\mathcal{J}$ measures how well v approximates the values $\mathcal{Z}$ over the set of points $\mathcal{P}$ (in the least squares sense), while the second and the third ones represent the *minimal energy condition*. These last two terms are included in the functional $\mathcal{J}$ in order to dispose of a certain fairness control: recall that the semi-norms $|\cdot|_1$ and $|\cdot|_2$ can be seen as a simplified measure of the surface area and of the bending energy, respectively. The *smoothing parameters* τ_1 and τ_2 weight the importance given to each of the two semi-norms. The optimal values of these parameters are discussed in [17].

Hence, given a Δ^1-triangulation $\mathcal{T}$ of $\overline{D}$ and its associated Powell-Sabin triangulation $\mathcal{T}_6$, the problem we consider is:

Problem 1. *We look for an element*

$$\sigma \in \mathcal{S}_2^1(D, \mathcal{T}_6)$$

such that

$$\mathcal{J}(\sigma) \leq \mathcal{J}(v) \quad \textit{for all} \quad v \in \mathcal{S}_2^1(D, \mathcal{T}_6).$$

In Proposition 1 of [18] it is shown that *Problem 1* has a unique solution which is also the unique solution of the following variational problem:

Problem 2. *Find* $\sigma \in \mathcal{S}_2^1(D, \mathcal{T}_6)$ *such that*

$$< \rho(\sigma),\, \rho(v) >_q + \tau_1(\sigma,\, v)_{1,D} + \tau_2(\sigma,\, v)_{2,D} =< \mathcal{Z},\, \rho(v) >_q \tag{2}$$

holds for all $v \in \mathcal{S}_2^1(D, \mathcal{T}_6)$.

Let N be the dimension of $\mathcal{S}_2^1(D, \mathcal{T}_6)$ -by the existence and uniqueness property stated in Remark 1, we know that $N = 3\#(\mathcal{Z}_\mathcal{T})$- and let $\{w_1, \ldots, w_N\}$ be any basis of the space $\mathcal{S}_2^1(D, \mathcal{T}_6)$. After some algebraic calculations, it can be checked (see the details in [18]) that the solution of the variational problem (2) is

$$\sigma = \sum_{i=1}^{N} \alpha_i w_i,$$

where the coefficients $\boldsymbol{\alpha} = (\alpha_1, \ldots, \alpha_N)$ can be obtained as the unique solution of the linear system

$$\boldsymbol{A}\boldsymbol{\alpha} = \boldsymbol{b},$$

where

$$\boldsymbol{A} = \left(< \rho(w_i),\, \rho(w_j) >_q + \sum_{m=1}^{2} \tau_m(w_i,\, w_j)_{m,D} \right)_{i,j=1}^{N} \quad \text{and}$$

$$\boldsymbol{b} = (< \mathcal{Z}, \rho(w_i) >_q)_{i=1}^{N}.$$

3. Formulation of the problem and main results

In this section, firstly we shall give some notations that we need for the statement of the problem of filling the original surface. Then, we split the problem into two steps by constructing in each of them a surface by minimizing a certain variational problem. The existence and uniqueness are proved in both stages. The last part of the section is devoted to the computation of the coefficients needed to construct the surface obtained in the second step.

Next we introduce some notation that will be used throughout the work:

- ▷ Let H (the hole) be a connected and nonempty subset of D (Figure 4, left) such that $Fr(D) \cap Fr(H) = \varnothing$, where $Fr(X)$ stands for the boundary of the set X. If H were not connected, the techniques given in this work to fill one connected hole would be applied to each of the connected components of H.

- ▷ Let $\mathcal{T}$ be a Δ^1-type triangulation of $\overline{D}$ with associated Powell-Sabin triangulation $\mathcal{T}_6$.

- ▷ Let $\mathcal{T}_H = \{T \in \mathcal{T} : T \cap H \neq \varnothing\}$ and $H^* = \bigcup_{T \in \mathcal{T}_H} T$. It is clear that H^* is a polygonal domain surrounding H (Figure 4, middle). We need to consider the Δ^1-type triangulation $\mathcal{T}$ fine enough to have $Fr(D) \cap Fr(H^*) = \varnothing$.

- ▷ Let $\mathcal{V}_\mathcal{T} = \{t_1, \ldots, t_s\}$ be the set of all the vertices of $\mathcal{T}$ laying on the boundary of H^* (Figure 4, right).

▷ Let

$$\mathcal{T}_{D-H^*} = \{T \in \mathcal{T} : T \subset D - H^*\}$$

and

$$(\mathcal{T}_{D-H^*})_6 = \{T \in \mathcal{T}_6 : T \subset D - H^*\}.$$

It is clear that $\mathcal{T}_{D-H^*}$ is a Δ^1-type triangulation of $\overline{D} - \overset{\circ}{H}{}^*$ with associated Powell-Sabin subtriangulation $(\mathcal{T}_{D-H^*})_6$.

▷ Analogously, let

$$\mathcal{T}_{H^*} = \{T \in \mathcal{T} : T \subset H^*\}$$

and

$$(\mathcal{T}_{H^*})_6 = \{T \in \mathcal{T}_6 : T \subset H^*\}.$$

It is clear that $\mathcal{T}_{H^*}$ is a Δ^1-type triangulation of H^* with associated Powell-Sabin subtriangulation $(\mathcal{T}_{H^*})_6$.

160 ▷ Let $f : \overline{D} - H \longrightarrow \mathbb{R}$ be a function.

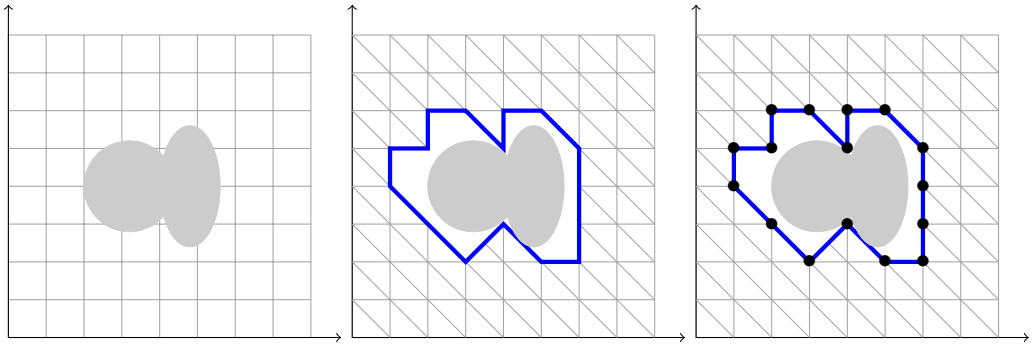

Figure 4: Hole H and surrounding H^*.

In addition, let us consider the functional vector spaces:

▷ $W_{D-H^*} = \left\{v|_{D-H^*} : v \in \mathcal{S}_2^1(D, \mathcal{T}_6)\right\}$,

▷ $W_{H^*} = \left\{v|_{H^*} : v \in \mathcal{S}_2^1(D, \mathcal{T}_6)\right\}$.

It can be easily shown that

$$W_{D-H^*} = \mathcal{S}_2^1\left(D - H^*, (\mathcal{T}_{D-H^*})_6\right)$$

and

$$W_{H^*} = \mathcal{S}_2^1\left(H^*, (\mathcal{T}_{H^*})_6\right).$$

We will denote $\mathcal{B}_{H^*}$ the usual Hermite basis of W_{H^*} associated with the knots of $\mathcal{T}$ belonging to H^*.

In order to 'fill' the hole in the graphic of f over H, and taking into account that we are interested in working with spline functions defined over triangulations, in what follows we will extend the hole H to H^*, i. e., we will consider the hole to be the surrounding H^* instead of H. Clearly, H^* tends to H as $diam(\mathcal{T}) \to 0$.

The problem that we pose is:

Problem 3. *We want to 'fill' the hole in the graphic of f over H^*, that is, we want to define a global reconstructed function*

$$\begin{array}{rcl} \widetilde{f} : D & \longrightarrow & \mathbb{R} \\ \boldsymbol{x} & \mapsto & \left\{ \begin{array}{ll} s_f & \text{if} \quad \boldsymbol{x} \in D - H^* \\ \sigma_{s_f} & \text{if} \quad \boldsymbol{x} \in H^* \end{array} \right. \end{array}$$

in such a way that:

i) $\widetilde{f} = s_f$ be as close as possible to f in $D - H^*$;

ii) $\widetilde{f} = \sigma_{s_f}$ fills the hole of f over H^* with a method based on one-dimension filling in such a way that σ_{s_f} be a kind of wireframe surface and the global reconstructed function $\widetilde{f}$ be of class $\mathcal{C}^1$.

To get this aim, we will proceed in two steps:

- ***Step 1: Construction of s_f.***

  In order to define s_f, let $\mathcal{P} = \{p_i\}_{i=1}^q$ be a subset of points in $\overline{D} - \overset{\circ}{H^*}$. Then, there exists ([18], Proposition 1) a unique $s_f \in W_{D-H^*}$ minimizing the functional

  $$\mathcal{J}_1 : W_{D-H^*} \longrightarrow \mathbb{R} \tag{3}$$

  defined by

  $$\mathcal{J}_1(v) = < \rho(v - f) >_q^2 + \lambda_1 |v|_{1,D-H^*}^2 + \lambda_2 |v|_{2,D-H^*}^2,$$

  where $\lambda_1 \geq 0, \lambda_2 > 0$ and ρ is the evaluation operator defined in (1).

  Observe that functions in W_{D-H^*} are splines globally $\mathcal{C}^1$ defined as the union of second order polynomial patches over each triangle of the triangulation $\mathcal{T}_6$, so that they are globally $\mathcal{H}^2$. As shown in Subsection 2.3, the unique s_f can be expressed as

  $$s_f = \sum_{i=1}^{\ell} \beta_i \gamma_i,$$

where $\{\gamma_1, \ldots, \gamma_\ell\}$ is a basis of W_{D-H^*} and $\boldsymbol{\beta} \equiv (\beta_i)_{i=1}^{\ell}$ is the solution of the linear system $\boldsymbol{A}\boldsymbol{\beta} = \boldsymbol{b}$, where

$$\boldsymbol{A} = \left(< \rho(\gamma_i), \rho(\gamma_j) >_q + \sum_{m=1}^{2} \lambda_m (\gamma_i, \gamma_j)_{m, D-H^*} \right)_{i,j=1}^{\ell}$$

and

$$\boldsymbol{b} = (< \rho(f), \rho(\gamma_i) >_q)_{i=1}^{\ell} .$$

Remark 2. *The quality of the fitting s_f (i. e., the degree of closeness of s_f to the original f over $\overline{D} - \overset{\circ}{H}{}^*$) depends on several aspects among which we find the cardinal and the density of the points in set $\mathcal{P}$. A very precise and technical result on this topic can be found in Theorem 5 of [18]. In the examples considered in the final section, $\mathcal{P}$ consists of* 2500 *random points in $\overline{D} - \overset{\circ}{H}{}^*$. Empirical results show that such an amount of points lead to good-quality fitting surfaces.*

- ***Step 2: Construction of σ_{s_f}.***

  Now, we obtain the filling function σ_{s_f}. In order to do that, first we consider in the domain $\mathring{H}^*$ a net of curves in two parametric directions. Then, we map all these planar curves into the space by means of a smooth function and by taking a set of points of the resulting family we finally construct σ_{s_f}.

  Let $a = \min\{x : (x, y) \in \overline{D}\}$ and $b = \max\{x : (x, y) \in \overline{D}\}$ and let us consider a partition

$$\{a = x_0 < x_1 < \cdots < x_n = b\} \tag{4}$$

  of $[a, b]$. Analogously, let $c = \min\{y : (x, y) \in \overline{D}\}$ and $d = \max\{y : (x, y) \in \overline{D}\}$ and let us consider a partition

$$\{c = y_0 < y_1 < \cdots < y_m = d\} \tag{5}$$

  of $[c, d]$.

  Let us consider the set $\mathcal{P}_x = \{X_p\}_{p=1}^{n_x}$ of all connected components with non-empty interior of the set

$$\left(\bigcup_{i=1}^{n-1} \{(x_i, y) \in D\} \right) \cap H^* .$$

Let c_p, d_p, with $c < c_p < d_p < d$ and for $p = 1, \ldots, n_x$, be such that $X_p = \{(x_{i(p)}, y) : y \in [c_p, d_p]\}$ with $i(p) \in \{1, \ldots, n-1\}$.

Analogously, let us consider the set $\mathcal{P}_y = \{Y_q\}_{q=1}^{n_y}$ of all connected components with non-empty interior of the set

$$\left(\bigcup_{j=1}^{m-1} \{(x, y_j) \in D\} \right) \cap H^*,$$

and let a_q, b_q, with $a < a_q < b_q < b$ and for $q = 1, \ldots, n_y$, be such that $Y_q = \{(x, y_{j(q)}) : x \in [a_q, b_q]\}$ with $j(q) \in \{1, \ldots, m-1\}$.

For $i = 1, \ldots, n-1$ and for $j = 1, \ldots, m-1$, let f_{x_i} and f_{y_j} be the univariate functions

$$f_{x_i}(y) = f(x_i, y) \quad \text{for } (x_i, y) \in \overline{D} - H^*$$

and

$$f_{y_j}(x) = f(x, y_j) \quad \text{for } (x, y_j) \in \overline{D} - H^*.$$

For $p = 1, \ldots, n_x$ and for $q = 1, \ldots, n_y$, let

$$f_p^* : X_p \longrightarrow \mathbb{R} \quad \text{and} \quad g_q^* : Y_q \longrightarrow \mathbb{R}$$

be the univariate functions filling the hole of $f_{x_{i(p)}}$ and $g_{y_{j(q)}}$ over X_p and over Y_q, respectively.

In the examples shown in this paper, we use two different method to fill univariate functions using low degree interpolation polynomials.

In order to obtain the filling function σ_{s_f} of Step 2, we will consider an appropriate subset $\mathcal{W} \subset W_{H^*}$, chosen in such a way that the global filling function $\widetilde{f}$ be of class $\mathcal{C}^1$, and an appropriate functional $\mathcal{J}_2$ defined in $\mathcal{W}$ to be minimized:

Let us consider the map

$$\varphi(v) = (\varphi_i(v))_{i=1}^{3s} \qquad \text{for } v \in W_{H^*},$$

where

$$\begin{cases} \varphi_i(v) = v(t_i) \\ \varphi_{s+i}(v) = \dfrac{\partial v}{\partial x}(t_i) \\ \varphi_{2s+i}(v) = \dfrac{\partial v}{\partial y}(t_i) \end{cases} \qquad \text{for } i = 1, \ldots, s.$$

Then, the functional spline space considered is

$$\mathcal{W} = \{v \in W_{H^*} : \varphi(v) = \varphi(s_f)\}.$$

205 That is, we will consider the functions of W_{H^*} such that their values and the ones of their first partial derivatives coincide in the knots of $\mathcal{V}_{\mathcal{T}}$ with those of the function s_f defined in Step 1. In such a way, $\widetilde{f}$ will be of class $\mathcal{C}^1$.

On the other hand, the functional $\mathcal{J}_2$ considered will be

$$\mathcal{J}_2 : \mathcal{W} \longrightarrow \mathbb{R} \tag{6}$$

defined by

$$\mathcal{J}_2(v) = \sum_{q=1}^{n_y} \int_{Y_q} \left(v - g_q^*\right)^2 dx + \sum_{p=1}^{n_x} \int_{X_p} \left(v - f_p^*\right)^2 dy + \tau_1 |v|^2_{1,H^*} + \tau_2 |v|^2_{2,H^*} =$$
$$\sum_{q=1}^{n_y} \int_{a_q}^{b_q} \left(v\left(x, y_{j(q)}\right) - g_q^*(x)\right)^2 dx + \sum_{p=1}^{n_x} \int_{c_p}^{d_p} \left(v\left(x_{i(p)}, y\right) - f_p^*(y)\right)^2 dy +$$
$$+ \tau_1 |v|^2_{1,H^*} + \tau_2 |v|^2_{2,H^*},$$

where $\tau_1 \geq 0, \tau_2 > 0$

Theorem 4. *There exists a unique $\sigma_{s_f} \in \mathcal{W}$ minimizing the functional $\mathcal{J}_2$ which is also the solution of the following variational problem:*

$$\begin{cases} \text{Find } \sigma_{s_f} \in \mathcal{W} \text{ such that} \\ \displaystyle\sum_{q=1}^{n_y} \int_{a_q}^{b_q} \sigma_{s_f} \cdot v\left(x, y_{j(q)}\right) dx + \sum_{p=1}^{n_x} \int_{c_p}^{d_p} \sigma_{s_f} \cdot v\left(x_{i(p)}, y\right) dy + \sum_{m=1}^{2} \tau_m (\sigma_{s_f}, v)_{m,H^*} \\ \qquad = \displaystyle\sum_{q=1}^{n_y} \int_{a_q}^{b_q} g_q^*(x) \cdot v\left(x, y_{j(q)}\right) dx + \sum_{p=1}^{n_x} \int_{c_p}^{d_p} f_p^*(y) \cdot v\left(x_{i(p)}, y\right) dy \\ \text{for all } v \in \mathcal{W}^0 = \{v \in W_{H^*} : \varphi(v) = \mathbf{0}\}. \end{cases} \tag{7}$$

Proof. Let $\{k_1, k_2, k_3\}$ be a $\mathbb{P}_1$-unisolvent subset of $\mathcal{V}_{\mathcal{T}}$. It is then easy to check that the map $[[\cdot]]_{H^*} : W_{H^*} \longrightarrow \mathbb{R}$ defined by

$$[[v]]_{H^*} = \left(\sum_{i=1}^{3} v(k_i)^2 + \tau_2 |v|^2_{2,H^*} \right)^{1/2}$$

defines a semi-norm on W_{H^*}. Besides, if $[[v]]_{H^*} = 0$, then v is a polynomial of total degree at most one vanishing at three non colinear points, and thus $v = 0$. Then, $[[v]]_{H^*}$ defines a norm on the finite dimensional space W_{H^*}

equivalent to the usual norm $\|v\|_{H^*} = \left(\sum_{|\beta|\leq 2} \int_{H^*} \partial^\beta v(x)^2 dx\right)^{1/2}$ and, as a consequence, the map $a : W_{H^*} \times W_{H^*} \longrightarrow \mathbb{R}$ defined by

$$a(u,v) = \\ 2\left(\sum_{i=1}^{3} u(k_i)v(k_i) + \sum_{q=1}^{n_y}\int_{a_q}^{b_q} u\cdot v\left(x, y_{j(q)}\right)dx + \sum_{p=1}^{n_x}\int_{c_p}^{d_p} u\cdot v\left(x_{i(p)}, y\right)dy \right. \\ \left. + \sum_{m=1}^{2}\tau_m(u,v)_{j,H^*}\right)$$

is a bilinear, continuous, symmetric and W_{H^*}-elliptic form. On the other hand, the map $\psi : W_{H^*} \longrightarrow \mathbb{R}$ defined by

$$\psi(v) = 2\left(\sum_{q=1}^{n_y}\int_{a_q}^{b_q} g_q^*(x)\cdot v\left(x, y_{j(q)}\right)dx + \sum_{p=1}^{n_x}\int_{c_p}^{d_p} f_p^*(y)\cdot v\left(x_{i(p)}, y\right)dy\right)$$

is a linear and continuous form. Hence, by applying the Stampacchia Theorem we find that there exists a unique $\sigma_{s_f} \in \mathcal{W}$ such that $a(\sigma_{s_f}, w - \sigma_{s_f}) \geq \psi(w - \sigma_{s_f})$ for all $w \in \mathcal{W}$. Hence, $a(\sigma_{s_f}, v) \geq \psi(v)$ for all $v \in \mathcal{W}^0$. But since $-v \in \mathcal{W}^0$, then $a(\sigma_{s_f}, v) = \psi(v)$ for all $v \in \mathcal{W}^0$, from which we obtain (7).

Moreover, σ_{s_f} is the minimum in $\mathcal{W}$ of the functional

$$\frac{1}{2}a(v,v) - \psi(v) = \mathcal{J}_2(v) + \sum_{i=1}^{3} s_f(k_i)^2 - \sum_{q=1}^{n_y}\int_{a_q}^{b_q} g_q^*(x)^2 dx - \sum_{p=1}^{n_x}\int_{c_p}^{d_p} f_p^*(y)^2 dy,$$

and thus σ_{s_f} also minimizes $\mathcal{J}_2$.

□

Remark 3. *In order to compute σ_{s_f} verifying (7), let us consider the usual Hermite basis $\mathcal{B}_{\partial H^*} = \{w_i\}_{i=1}^{3s}$ associated with the knots in $\mathcal{V}_\mathcal{T}$, that is, the ones verifying $\varphi(w_i) = (0,\ldots,0,\overset{i)}{1},0,\ldots,0)$ for all $i \in \{1,\ldots,3s\}$, and let us extend $\mathcal{B}_{\partial H^*}$ to the usual Hermite basis*

$$\mathcal{B}_{H^*} = \{w_1,\ldots,w_{3s},w_{3s+1},\ldots,w_n\}$$

of W_{H^*}, in such a way that $\{w_{3s+1},\ldots,w_n\}$ is a basis of $\mathcal{W}^0$. Then, the fact that $\sigma_{s_f} \in \mathcal{W}$ together with equations (7) lead to the expression

$$\sigma_{s_f} = \sum_{i=1}^{3s}\varphi_i(s_f)w_i + \sum_{j=3s+1}^{n}\alpha_{j-3s}w_j \equiv \widehat{\sigma}_{s_f} + \widehat{\sigma}_{s_0},$$

where the vector $(\alpha_j)_{j=1}^{n-3s}$ *is the solution of the linear equations system*

$$(\mathcal{I}+\mathcal{R})\,x=\mathcal{S}+\mathcal{K}+\mathcal{Q},$$

being:

$$\mathcal{I}=\left(\sum_{q=1}^{n_y}\int_{a_q}^{b_q} w_j\cdot w_t\left(x,y_{j(q)}\right)dx+\sum_{p=1}^{n_x}\int_{c_p}^{d_p} w_j\cdot w_t\left(x_{i(p)},y\right)dy\right)_{j,t=3s+1}^{n};$$

$$\mathcal{R}=(\tau_1(w_j,w_t)_{1,H^*}+\tau_2(w_j,w_t)_{2,H^*})_{j,t=3s+1}^{n};$$

$$\mathcal{S}=\left(\sum_{q=1}^{n_y}\int_{a_q}^{b_q} g_q^*(x)\cdot w_t\left(x,y_{j(q)}\right)dx+\sum_{p=1}^{n_x}\int_{c_p}^{d_p} f_p^*(y)\cdot w_t\left(x_{i(p)},y\right)dy\right)_{t=3s+1}^{n};$$

$$\mathcal{K}=-\sum_{i=1}^{3s}\varphi_i(s_f)\left(\sum_{q=1}^{n_y}\int_{a_q}^{b_q} w_i\cdot w_t\left(x,y_{j(q)}\right)dx+\sum_{p=1}^{n_x}\int_{c_p}^{d_p} w_i\cdot w_t\left(x_{i(p)},y\right)dy\right)_{t=3s+1}^{n};$$

$$\mathcal{Q}=-\sum_{i=1}^{3s}\varphi_i(s_f)\left(\tau_1(w_i,w_t)_{1,H^*}+\tau_2(w_i,w_t)_{2,H^*}\right)_{t=3s+1}^{n}.$$

If we rewrite the variational formulation (7) in terms of $\widehat{\sigma}_{s_0}=\sigma_{s_f}-\widehat{\sigma}_{s_f}\in\mathcal{W}^0$ *then we could also reformulate the proof of Theorem 4 in terms of the more well-known Lax-Milgram lemma instead of the more general Stampacchia theorem.*

Remark 4. *We must note that the two stages of the scheme developed in Step 2 to fill surfaces enjoy a measure of independence. Namely, the way considered in the first stage to obtain* f_p^* *and* g_q^* *can be defined based on the particular* f_{x_i} *and* g_{y_j} *to be fill and/or on the particular shape we may want the fillings* f_p^* *and* g_q^* *to have. Later, second stage to obtain* σ_{s_f} *can be carried out whatever the method to obtain* f_p^* *and* g_q^* *be. Nevertheless, the shape and quality of the final reconstructed* σ_{s_f} *of course will strongly depend on the results of* f_p^* *and* g_q^* *.*

4. Numerical and graphical examples

To illustrate the method developed in this paper, we show in this section different numerical and graphical tests. Subsection 4.1 is devoted to examples over uniform wireframe meshes, Subsection 4.2 to examples over non-uniform ones, and in Subsection 4.3 we consider a different $1D$-filling scheme from the one used in Subsections 4.1 and 4.2 to implement first stage of Step 2. In all cases, we have taken the data:

- The domain $D=(0,1)\times(0,1)$.
- For different values of n, the Δ^1-type triangulation $\mathcal{T}^n$ of $\overline{D}$ associated to the uniform partition of each side of D into n sub-intervals (see Figure 5, left).

- The smoothing parameters $\lambda_1 = 10^{-3}; \lambda_2 = 10^{-6}$ in functional $\mathcal{J}_1$ (see (3)). The raison to use such values is that in previous works based on the same functional to fit a dataset it has been checked that these are 'good' values of the smoothing parameters to obtain a proper fitting surface. On the other hand, in order to give the same weights to semi-norms $|\cdot|_1$ and $|\cdot|_2$ inside and outside the hole, we have taken $\tau_1 = 10^{-3}$ and $\tau_2 = 10^{-6}$ in functional $\mathcal{J}_2$ (see (6)).

- A subset $\mathcal{P}$ of points consisting in 2500 random points in $\overline{D} - \overset{\circ}{H^*}$ in order to consider functional $\mathcal{J}_1$ (3).

- The test functions:

  - Sinusoidal: $f^1(x,y) = \sin\left(2\pi^2\,(x-0.5)\,(y-0.5)\right)$;
  - Semisphere:

$$f^2(x,y) = \begin{cases} \sqrt{0.5^2 - (x-0.5)^2 - (y-0.5)^2} & \text{if} \quad (x-0.5)^2 + (y-0.5)^2 \leq 0.5^2 \\ 0 & \text{otherwise} \end{cases};$$

  - Franke's function:

$$f^3(x,y) = 0.75e^{-\frac{(9y-2)^2+(9x-2)^2}{4}} + 0.75e^{-\frac{(9y+1)^2}{49} - \frac{(9x+1)}{10}} + 0.5e^{-\frac{(9y-7)^2+(9x-3)^2}{4}} - 0.2e^{-\left((9y-4)^2+(9x-7)^2\right)};$$

  - Nielson's function: $f^4(x,y) = \frac{y}{2} cos^4\left(4(x^2+y-1)\right)$.

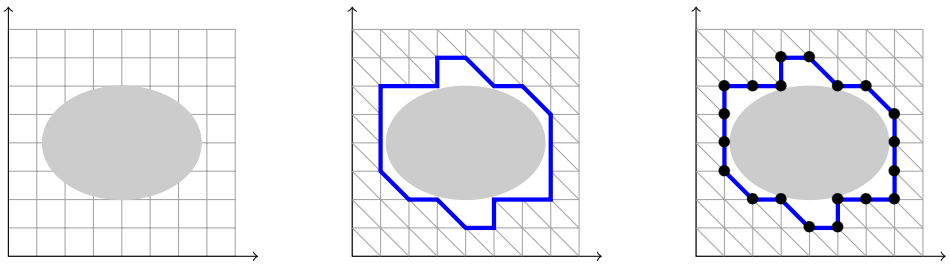

Figure 5: Triangulation $\mathcal{T}^8$, hole H and polygonal hole H^*.

As explained in Remark 4, we must note that the final stage of obtaining the filling function by minimizing the functional $\mathcal{J}_2$ is, in some sense, independent from the way used to obtain the filled f_p^* and g_q^*, so that in every example we can decide which $1D$-filling scheme we want to use, although of course different techniques used to calculate f_p^* and g_q^* will give different σ_{s_f} functions. In this numerical and graphical section we will work with two different $1D$-filling schemes: an

interpolation scheme, which will be used in Subsections 4.1 and 4.2, and a mixed interpolation-fitting scheme, that will be explained and used in Subsection 4.3. The one used in Subsections 4.1 and 4.2 comprises interpolation using polynomials of fifth degree: For every connected component $X_p = \{(x_{i(p)}, y) : y \in [c_p, d_p]\}$, we define the f_p^* function inside X_p so that it is $\mathcal{C}^2$ with the definition given by $f_{x_i(p)}(y) \equiv f(x_i(p), y)$ in $\overline{D} - H^*$. Namely, we have considered $f_p^*|_{X_p}$ to be the fifth degree polynomial verifying

$$\begin{aligned} f_p^*|_{X_p}(c_p) &= f_{x_i(p)}(c_p) & f_p^*|_{X_p}(d_p) &= f_{x_i(p)}(d_p), \\ f_p^*|_{X_p}{}'(c_p) &= f'_{x_i(p)}(c_p) & f_p^*|_{X_p}{}'(d_p) &= f'_{x_i(p)}(d_p), \\ f_p^*|_{X_p}{}''(c_p) &= f''_{x_i(p)}(c_p) & f_p^*|_{X_p}{}''(d_p) &= f''_{x_i(p)}(d_p). \end{aligned} \tag{8}$$

Analogously, for every connected component $Y_q = \{(x, y_{j(q)}) : x \in [a_q, b_q]\}$, we consider g_q^* so that $g_q^*|_{Y_q}$ is the fifth degree polynomial verifying

$$\begin{aligned} g_q^*|_{Y_q}(a_q) &= f_{y_j(q)}(a_q) & g_q^*|_{Y_q}(b_q) &= f_{y_j(q)}(b_q), \\ g_q^*|_{Y_q}{}'(a_q) &= f'_{y_j(q)}(a_q) & g_q^*|_{Y_q}{}'(b_q) &= f'_{y_j(q)}(b_q), \\ g_q^*|_{Y_q}{}''(a_q) &= f''_{y_j(q)}(a_q) & g_q^*|_{Y_q}{}''(b_q) &= f''_{y_j(q)}(b_q). \end{aligned} \tag{9}$$

Observe that all these interpolation problems are clearly unisolvent, require little computational work and, as we will see, lead to good results.

4.1. Examples over uniform wireframe meshes

First of all we present several examples constructed over uniform wireframe meshes, i. e., partitions verifying $x_i - x_{i-1} = \frac{1}{n}$ for $i = 1, \ldots, n$ and $y_j - y_{j-1} = \frac{1}{m}$ for $j = 1, \ldots, m$, with the notation introduced in (4) and (5).

We have considered H to be the hole defined implicitly (see Figure 5, middle) by

$$\frac{\left(x - \frac{1}{2}\right)^2}{0.35^2} + \frac{\left(y - \frac{1}{2}\right)^2}{0.25^2} \leq 1$$

and the Δ^1-triangulation $\mathcal{T}^8$ of $\overline{D}$.

In Figure 6 we show: in the first row, the graphics of the original test functions f^k (for $k = 1, 2, 3$); in the second row, the graphics of f^k with the hole and of the functions $f_{x_i}^k$ and $g_{y_j}^k$ over $\overline{D} - H$; in the third row, the graphics of $f_{x_i}^k$ and $g_{y_j}^k$ over $\overline{D} - H^*$ (blue) together with the graphics of the filled f_p^{k*} and g_q^{k*} inside H^* (yellow) and, finally, in the last row, we show the graphics of the reconstructed $\widetilde{f^k}$ together with the filling functions f_p^{k*} and g_q^{k*} used to obtain σ_{f^k}. The density of the wiferame meshes considered to obtain the reconstructed $\widetilde{f^k}$ have been $n = 5, m = 6$ for the test function f^1; $n = 10, m = 15$ for the test function f^2 and $n = 20, m = 25$ for the test function f^3.

In order to "quantify" the kindness of the filling function, we have estimated the L^2-relative error of the reconstructed $\widetilde{f^k}$ outside and inside the hole (E_{out} and E_{in}, respectively) by means of the formulas

$$E_{out} = \left(\frac{\sum_{i=1}^{2500} (f^k(a_i) - s_{f^k}(a_i))^2}{\sum_{i=1}^{2500} f^k(a_i)^2} \right)^{1/2} ; E_{in} = \left(\frac{\sum_{i=1}^{2500} (f^k(b_i) - \sigma_{s_{f^k}}(b_i))^2}{\sum_{i=1}^{2500} f^k(b_i)^2} \right)^{1/2},$$

where $\{a_i\}_{i=1}^{2500}$ are random points in $\overline{D} - \overset{\circ}{H}{}^*$ and $\{b_i\}_{i=1}^{2500}$ are random points in H^*. We have also estimated the relative maximum error of $\widetilde{f^k}$ inside the hole:

$$E_{max} = \frac{\max_i \left| f^k(c_i) - \sigma_{s_{f^k}}(c_i) \right|}{\max_i |f^k(c_i)|}$$

where $\{c_i\}_{i=1}^{2500}$ are random points in H^*. In Figure 6 we also include these errors for the test functions considered.

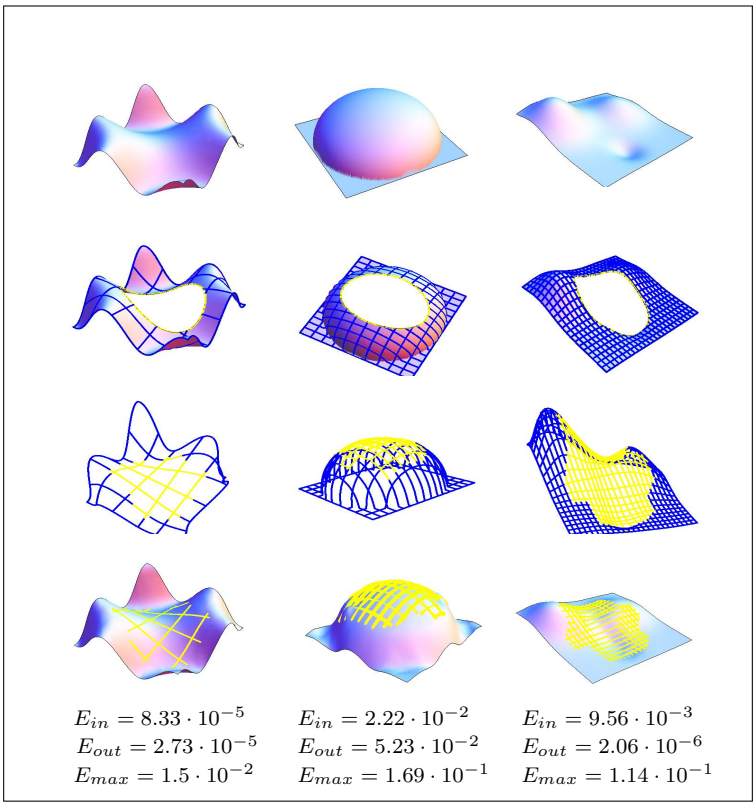

Figure 6: Filling surfaces over uniform wireframe meshes.

Next we consider (Figure 7) the test function f^4 over the very fine wireframe mesh $m = n = 50$:

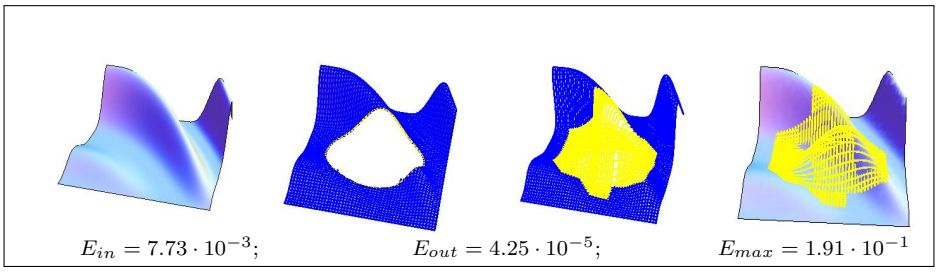

Figure 7: Filling surfaces over uniform wireframe meshes.

4.2. Examples over non-uniform wireframe meshes

Next we present several examples carried out over non-uniform wireframe meshes. First, we fill Franke's function over the hole $H \equiv \frac{\left(x-\frac{1}{2}\right)^2}{0.4^2} + \frac{\left(y-\frac{1}{2}\right)^2}{0.15^2} \leq 1$ and the triangulation $\mathcal{T}^{15}$ (Figure 8, left). The wireframe mesh considered has been (Figure 8, middle):

$$\begin{aligned} \{x_i\}_{i=1}^{n-1} &= \left\{\frac{1}{2} - 0.4 + \frac{0.4}{2^k}\right\}_{k=1}^{5} \bigcup \left\{\frac{1}{2} + 0.4 - \frac{0.4}{2^k}\right\}_{k=1}^{5}; \\ \{y_j\}_{j=1}^{m-1} &= \left\{\frac{1}{2} - 0.15 + \frac{0.15}{2^k}\right\}_{i=k}^{5} \bigcup \left\{\frac{1}{2} + 0.15 - \frac{0.15}{2^k}\right\}_{k=1}^{5}. \end{aligned} \tag{10}$$

In Figure 8 right we show the segments X_p (red) and Y_q (green) over which the functions f_{x_i} and g_{y_j} must be, respectively, filled.

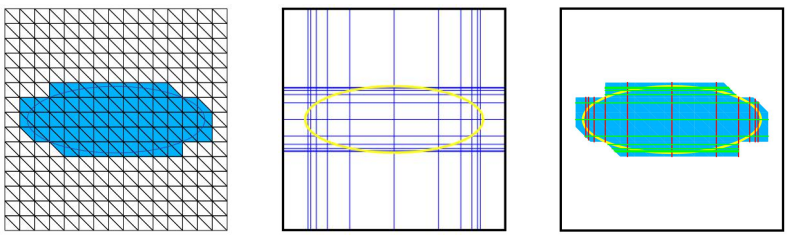

Figure 8: Graphics related to test function f^4.

The main reason to have considered such a hole H, such a triangulation $\mathcal{T}^{15}$ and such a wireframe mesh is to dispose of 'shorts' segments inside H^* to be filled in order that the filling of the functions f_{x_i} and g_{y_j} over the X_p and the Y_q, respectively, be more precise. In other words, our aim has been to concentrate most of wireframes near the boundary of the hole, where its 'width' is lower. The

expected result is to reconstruct the test function with higher degree of accuracy near the boundary of the hole to later fill in its interior with more accurate information. The results are quite good (a little bit better inside the hole that the ones obtained in the uniform wireframe mesh case), as shown in Figure 9:

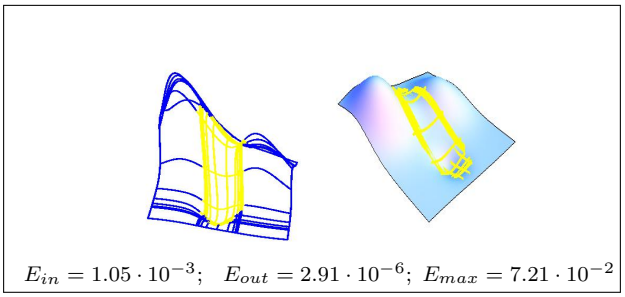

Figure 9: Filling surfaces over non-uniform wireframe meshes.

We have also considered Nielson's function over the hole $H \equiv \frac{\left(x-\frac{1}{2}\right)^2}{0.15^2} + \frac{\left(y-\frac{1}{2}\right)^2}{0.4^2} \leq 1$ and the wireframe mesh obtaining by interchanging the sets $\{x_i\}$ and $\{y_j\}$ in (10) (see Figure 10, left). The results are shown in Figure 10 (middle and right).

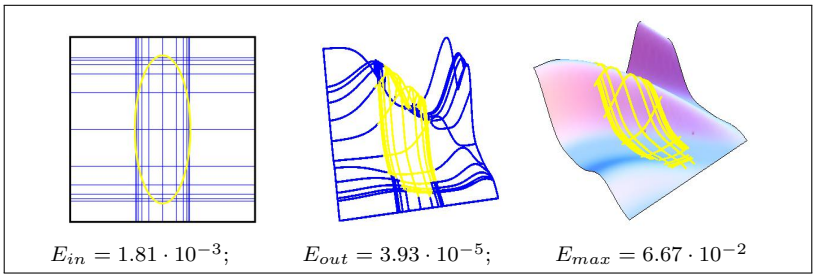

Figure 10: Filling surfaces over non-uniform wireframe meshes.

In the next example we have considered a kind of 'adaptive' non-uniform mesh constructed *ad hoc* to the surface to be filled: first, we have considered a uniform mesh with $n = 30$ and $m = 20$ (Figure 11, left); the hole defined in Subsection 4.1 and we have computed all the $1D$-filling functions f_p^* and g_q^* over the X_p and the Y_q, respectively. Let now $\mathcal{N}$ be the set of knots of the wireframe lying in H^*, i. e.:

$$\mathcal{N} = \{(x_i, y_j) : (x_i, y_j) \in H^*; i = 1, \ldots, n-1; j = 1, \ldots, m-1\}.$$

Then, for all $p = 1, \ldots, n_x$, we have considered the quantities

$$\mathcal{E}_p^x = \text{Mean}\left\{\left(f_p^*(x_{i(p)}, y_{j(q)}) - g_q^*(x_{i(p)}, y_{j(q)})\right)^2 : (x_{i(p)}, y_{j(q)}) \in \mathcal{N}\right\}_{q=1}^{n_y}$$

and, analogously, for all $q = 1, \ldots, n_y$, we have computed

$$\mathcal{E}_q^y = \text{Mean}\left\{\left(g_q^*(x_{i(p)}, y_{j(q)}) - f_p^*(x_{i(p)}, y_{j(q)})\right)^2 : (x_{i(p)}, y_{j(q)}) \in \mathcal{N}\right\}_{p=1}^{n_x}.$$

The idea of computing $\mathcal{E}_p^x$ (resp. $\mathcal{E}_q^y$) is to dispose of a 'kind of measure' of how the behaviour, the consistency of each filled f_p^* (resp. g_q^*) with all perpendicular filled g_q^* (resp. f_p^*) is, in such a way that we can remove from the original uniform wireframe all those leading to a 'non-coherent' behaviour with all the rest. More precisely, in the example considered, we have removed from functional (6) all wireframes X_p and Y_q associated to the 50% of highest values of $\mathcal{E}_p^x \cup \mathcal{E}_q^y$. In Figure 11 we show the graphics associated to an example carried out with Franke's function: in the second graphic we show the wireframes X_p and Y_q that we have not removed -i. e., the ones associated to the 50% of lowest values of $\mathcal{E}_p^x \cup \mathcal{E}_q^y$- (the interpretation of the third and fourth graphics is as in the previous examples).

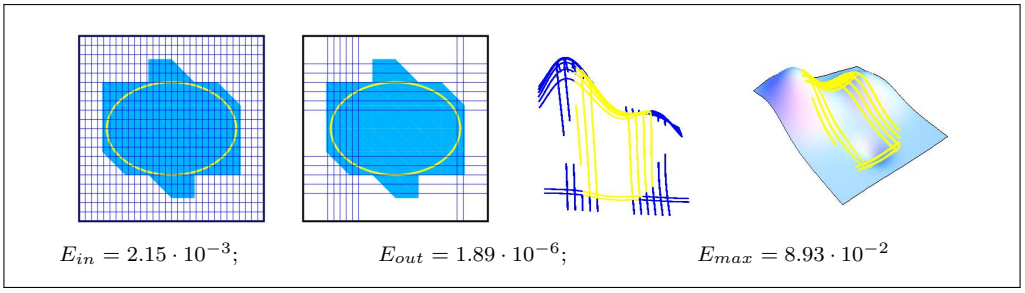

Figure 11: Filling surfaces over an 'adaptative' non-uniform wireframe mesh.

In this last example we can observe that most of the survivor wireframes are near the boundary of H^* -as we considered in the first examples of this subsection-, and that the error results are quite similar to those obtained in such non-uniform early examples and better than the ones obtained in the uniform case. So, it seems that choosing the wireframes near the boundary of the hole leads to better results. We find it reasonable since it is just in this region where the original function can be better reconstructed.

4.3. Example with another 1D-filling scheme

Next we work with another $1D$-filling scheme -different from (8)-(9)- to fill univariate functions using low degree polynomials. This second method involves fitting and interpolation. Again we calculate $f_p^*|_{X_p}$ and $g_q^*|_{Y_q}$ which are fifth degree polynomial, but every polynomial is imposed four interpolation restrictions and additional conditions to determine the two remaining coefficients. Namely,

f_p^* is a polynomial that verifies the interpolation conditions

$$f_p^*|_{X_p}(c_p) = f_{x_i(p)}(c_p), \qquad f_p^*|_{X_p}(d_p) = f_{x_i(p)}(d_p),$$
$$f_p^*|_{X_p}{}'(c_p) = f'_{x_i(p)}(c_p), \qquad f_p^*|_{X_p}{}'(d_p) = f'_{x_i(p)}(d_p),$$

and also better fits f in eighth non equidistant points outside the interval $[c_p, d_p]$ in the sense of least squares. Thus, we obtain a polynomial of degree up to five, but we don't need information of the second derivatives of f, contrary to the other method used. The construction of g_q^* is analogous. In Figure 12 we present an example with Franke's function carried out over the same hole and uniform wireframe mesh described in Subsection 4.1. We see that the results obtained with filling scheme are worse than the ones obtained with the interpolation $1D$-filling scheme.

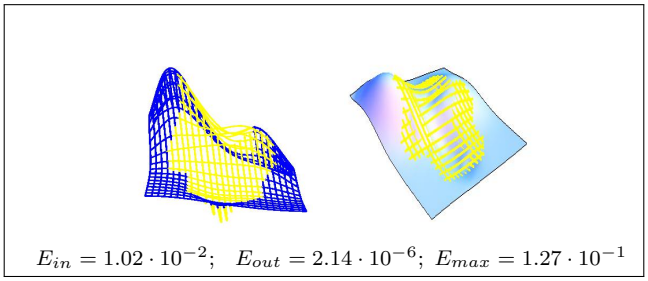

Figure 12: Filling surfaces over an interpolation-fitting $1D$-filling scheme.

Remark 5. *Observe that in this work, for sinusoidal and Nielson's functions we obtain relative errors inside the hole of order* 10^{-5} *and* 10^{-3}*, respectively, while with another filling methods (see e. g. [19]) the relative errors for these same test functions are of order* 10^{-3} *and* 10^{-2}*, respectively. In general, other filling methods lead to relative errors inside the hole of order* $10^{-2}/10^{-3}$ *for different test functions (see e. g. [20]), so, we can say that this new filling proposal is competitive.*

References

[1] J. C. Carr, R. K. Beatson, J. B. Cherrie, T. J. Mitchell, W. R. Fright, B. C. McCallum, T. R. Evans, Reconstruction and representation of 3D objects with radial basis functions, in: Proceedings of the 28th Annual Conference on Computer Graphics and Interactive Techniques, SIGGRAPH '01, ACM, New York, NY, USA, 2001, pp. 67–76. doi:10.1145/383259.383266.

[2] V. Caselles, G. Haro, G. Sapiro, J. Verdera, On geometric variational models for inpainting surface holes, Comput. Vis. Image Underst. 111 (3) (2008) 351–373. doi:10.1016/j.cviu.2008.01.002.

[3] L. Zi-Cai, Blending curves for landing problems by numerical differential equations, I. Mathematical modelling, Mathematical and Computer Modelling 31 (2) (2000) 161 – 177. doi:10.1016/S0895-7177(99)00230-7.

[4] M. A. Fortes, P. González, M. J. Ibáñez, M. Pasadas, Interpolating minimal energy $\mathcal{C}^1$-surfaces on Powell-Sabin triangulations. application to the resolution of elliptic problems, Num. Meth. Part. Diff. Equat. 31 (3) (2015) 798–821. doi:10.1002/num.21918.

[5] J. Hahn, Filling polygonal holes with rectangular patches, in: W. Straßer, H.-P. Seidel (Eds.), Theory and Practice of Geometric Modeling, Springer, Berlin, 1989, pp. 81–91. doi:10.1007/978-3-642-61542-9_6.

[6] C. K. Chui, M.-J. Lai, Filling polygonal holes using $\mathcal{C}^1$ cubic triangular spline patches, Computer Aided Geometric Design 17 (4) (2000) 297 – 307. doi:10.1016/S0167-8396(00)00005-4.

[7] D. Storry, A. Ball, Design of an n-sided surface patch from Hermite boundary data, Computer Aided Geometric Design 6 (2) (1989) 111 – 120. doi:10.1016/0167-8396(89)90014-9.

[8] E. Beeker, Smoothing of shapes designed with free-form surfaces, Computer Aided Design 18 (4) (1986) 224 – 232. doi:10.1016/0010-4485(86)90134-X.

[9] Y. Sergeyev, R. G. Strongin, D. Lera, Introduction to global optimization exploiting space-filling curves, Springer–Verlag, New York, 2013. doi:10.1007/978-1-4614-8042-6.

[10] H. Sagan, Space-Filling Curves, Springer–Verlag, New York, 1994. doi:10.1007/978-1-4612-0871-6.

[11] G. Farin, Curves and Surfaces in CAGD. A Practical Guide, 5th Edition, Morgan Kaufmann, 2002. doi:10.1016/B978-1-55860-737-8.X5000-5.

[12] M. A. Fortes, P. González, M. L. Rodríguez, M. Pasadas, A hole filling method for explicit and parametric surfaces by using $\mathcal{C}^1$-Powell-Sabin splines, Math. and Comp. in Simul. 99 (2014) 71–81. doi:10.1016/j.matcom.2013.04.013.

[13] O. V. Davydov, G. Nürnberger, F. Zeifelder, Approximation order of bivariate spline interpolation for arbitrary smoothness, J. Comput. Appl. Math. 90 (2) (1998) 117–134. doi:10.1016/S0377-0427(98)00004-1.

[14] M. Laghchim-Lahlou, P. Sablonnière, $\mathcal{C}^r$-finite elements of Powell-Sabin type on the three direction mesh, Adv. in Comput. Math. 6 (1) (1996) 191–206. doi:10.1007/BF02127703.

[15] M. J. D. Powell, M. A. Sabin, Piecewise quadratic approximations on triangles, ACM Trans. on Math. Softw. 3 (4) (1977) 316–325.

[16] P. Sablonnière, Error bounds for Hermite interpolation by quadratic splines on an α-triangulation, IMA J. of Numer. Anal. 7 (4) (1987) 495–508. doi:10.1093/imanum/7.4.495.

[17] D. Barrera, M. A. Fortes, P. González, M. Pasadas, Minimal energy $\mathcal{C}^r$-surfaces on uniform Powell-Sabin type meshes: Estimation of the smoothing parameters, Math. and Comp. in Simul. 77 (2-3) (2008) 161–169. doi:10.1016/j.matcom.2007.08.020.

[18] D. Barrera, M. A. Fortes, P. González, M. Pasadas, Minimal energy surfaces on Powell-Sabin type triangulations, Appl. Num. Math. 58 (5) (2008) 635–645. doi:10.1016/j.apnum.2007.02.001.

[19] D. Barrera, M. A. Fortes, P. González, M. Pasadas, Filling polygonal holes with minimal energy surfaces on Powell-Sabin type triangulations, J. Comput. Appl. Math. 234 (4) (2010) 1058–1068. doi:10.1016/j.cam.2009.04.012.

[20] M. A. Fortes, P. González, A. Palomares, M. Pasadas, Filling holes with shape preserving conditions, Math. and Comp. in Simul. 118 (2015) 198–212. doi:10.1016/j.matcom.2014.12.008.